5-1-2018

Shape Control of A Spatial Cable

Bo Tian
Lehigh University, thu_tb@qq.com

Shape Control of a Spatial Cable

by

Bo Tian

Presented to the Graduate and Research Committee

of Lehigh University

in Candidacy for the Degree of

Master of Science

in

Mechanical Engineering

Lehigh University

May 2018

Certification of Approval

This thesis is accepted and approved in partial fulfillment of the requirements for the Master of Science.

_____

Date

_____

Prof. Subhrajit Bhattacharya

Thesis Advisor

_____

Prof. Gary Harlow

Chair of Department of

Mechanical Engineering and Mechanics

Acknowledgements

I would like to express my deep gratitude to Professor Subhrajit Bhattacharya for his valuable and patient guidance. His tremendous academic support have helped me immensely in all the time of research and writing of this thesis.

I would like to thank the Department of Mechanical Engineering and Mechanics of Lehigh University for providing such a wonderful and unforgettable academic experience.

Finally, I wish to thank my parents and friends for their support and encouragement throughout my graduate studies.

Contents

List of Figures

Abstract

Unmanned Aerial Vehicles (UAVs) have been widely used in scientific, industrial and military applications. Rotorcrafts, such as quadcopters, are agile and versatile in their applications. However one of the biggest challenges with such UAVs is their limited battery life that make the flight time for a typical UAVs limited to twenty to thirty minutes for most practical purposes. A solution to this problem lies in the use of cables that tether the UAV to a power outlet for constant power supply. However, the cable needs to be controlled effectively in order to avoid obstacles or other UAVs. In this thesis, we develop methods for controlling the shape of a cable using actuation at one or both ends. We propose a discrete model for the spatial cable and derive the equations governing the cable dynamics for both force controlled system and position controlled system. We design a controller to control the shape of the cable to attain the desired shape and perform simulations under different conditions. Finally, we propose a quasi-static model for the spatial cable and discuss the stability of this system and the proposed controller.

Chapter 1

Introduction

1.1 Background

As the technology of Unmanned Aerial Vehicles (UAVs) develops at a rapid pace, the applications of UAVs are greatly diversifying. Nowadays, the applications of UAV have expanded to commercial, scientific, agricultural and other areas. It plays an important role in aerial photography, surveillance, agriculture and so on.

Rotorcrafts, such as quadcopters are agile, can hover in place and can operate in cluttered environments. Such UAVs are usually battery powered, and due to the high power consumption, the flight time of a typical UAV is limited to a less than an hour. Thus, for some applications it is desirable that the UAVs be tethered to a base using a wire or a cable for power supply and high-speed communication (Figure 1.1(a)). The wired UAVs do have longer battery life and can work for longer time, which is a big advantage. However the cable limits the motion of the UAV. When obstacles appear, the cable may be blocked by the obstacles restricting the UAV's motion. Adjusting the position of UAV manually is a slow and ineffective way to let the cable dodge the obstacles. Instead, it may be desirable to control the shape of the cable using motion of the UAV that would allow it to dodge the obstacles.

Motivated by this application, we develop a method for controlling the shape and posi-

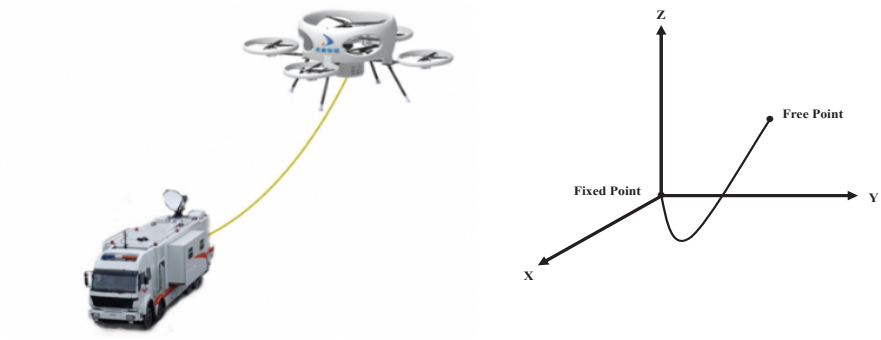

(a) An UAV tethered to a base. (b) The cable in three dimensions.

Figure 1.1: Tethered UAV.

tion of the cable using the motion of the UAV attached to it. One end of the cable is fixed at a base (e.g. a power outlet or communication base) and the other end is connected to the UAV ((Figure 1.1(b)). The cable deforms under the effects of gravity and UAV adjusts the position of cable by applying forces or adjusting the position of the end of the cable that it is connected to.

In this thesis, we develop a discrete model of a cable in order to simplify the problem. Then we develop a dynamic model and simulation with force and position control at the free end of the cable. We then develop a shape controller for the cable using the motion of the UAV as the input and evaluate the proposed controller both theoretically and through simulations.

1.2 Literature Review

Thee has been little to no prior research in tethered UAVs. However, there has been multiple studies on the modeling and simulation of a cable, none of which however explicitly consider the problem of controlling its scape.

Goriely and McMillen (2002) conducted a study on the shape of a cracking whip [1]. They built a dynamical model for the propagation and acceleration of waves in the motion of whips. Also, the respective contributions of tension, tapering, and boundary conditions

in the acceleration of an initial impulse are studied theoretically and numerically. Jimenez, Hernandez, Campos and Del-Valle (2005) studied the motion of a rope falling from a table [2]. They used Newtonian and canonical methods to analyze the problem.

Matsuno, Takayuki (2006) described configurations of ropes using a topological models and knot theory [3]. They also proposed a method to reconstruct the structure of a rope from sensor information through CCD cameras when a robot manipulates a rope and used that to perform slow manipulation experiments. In this thesis, we however consider highly dynamic rope shape manipulation, although we do not consider topological complexities such as knots.

Fritzkowski and Kaminski (2008) conducted two studies about modeling a rope as a rigid multibody system. In their first paper they considered the discrete model of a rope as a scleronomic and a rheonomic system [4]. They also performed numerical experiments and discussed the advantages of the applied algorithm on the basis of energy conservation. In their later study, Fritzkowski and Kaminski (2011) presented a discrete model of a rope to simulate the plane motion of the rope fixed at one end [5]. They presented two systems, whose members are rigid but non-ideal joints involve elasticity or dissipation.

Most of the above mentioned research deals with representation and modeling of ropes to understand their physics better with little or no consideration for control of the shape of the rope. Bhattacharya, Heidarsson, Sukhatme and Kumar (2011) studied the problem of shape control of a planar cable using robots attached to its two ends in context of oil skimming and cleanup operations [6]. They built a discrete model for the rope and simulated in 2 dimensions, where drag forces were considered. Additionally, they studied a quasi-static model and developed a shape controller based on it. In this thesis, we develop on the work of Bhattacharya et al. and extend the model to three spatial dimensions and thus propose shape controller for a highly dynamic model (as opposed to a quasi-static model). We use a quasi-static model for theoretical analysis though.

1.3 Preliminaries

1.3.1 Lagrangian Mechanics

Lagrangian mechanics is a reformulation of classical mechanics. Lagrangian mechanics is a convenient method that is widely used to solve dynamic problems. It allows one to choose a convenient set of generalized coordinates to simplify the problems and solve the equations of motion. In Newtonian mechanics, the equations of motion are given by Newton's second laws,

$$\sum \boldsymbol{F} = m\frac{\mathrm{d}^2\boldsymbol{r}}{\mathrm{d}t^2} \tag{1.1}$$

However, instead of forces, Lagrangian mechanics uses the energies in the system. The central quantity of Lagrangian mechanics is the Lagrangian. Lagrangian is a function of the generalized coordinates, their time derivatives, and time, and contains the information about the dynamics of the system.

Definition 1.3.1. ***Lagrangian*** *is defined as*

$$L = T - V \tag{1.2}$$

where T is the total kinetic energy and V is the total potential energy of the system.

If the system has one or more holonomic constraints, at any instant of time, the coordinates of a constrained particle are coupled and not independent. In this case, using variational principles we can derive the **Lagrange's equations of the first kind** [7].

Definition 1.3.2. ***Lagrange's equations of the first kind*** *is defined as*

$$\frac{\mathrm{d}}{\mathrm{d}t}\left(\frac{\partial \mathcal{L}}{\partial \dot{q}_l}\right) - \frac{\partial \mathcal{L}}{\partial q_l} - \sum_{i=1}^{C} \lambda_i \frac{\partial f_i}{\partial q_l} - Q_{q_l} = 0 \tag{1.3}$$

where q_l are the chosen generalized coordinates, C is the number of the constraint equations, λ_i are the Lagrange multiplier for each constraint equation f_i, and Q_{q_l} are the external

generalized forces.

Also, if we have total N generalized coordinates which are not independent, we can eliminate C coordinates in the equations to get $N - C$ independent coordinates using the constraint equations. We can transform each equation to a common set of this $N - C$ generalized coordinates and get the equations that do not include constraint forces at all. In this case, we can derive the **Lagrange's equations of the second kind** [7].

Definition 1.3.3. ***Lagrange's equations of the second kind (Euler - Lagrange equations)*** *is defined as*

$$\frac{\mathrm{d}}{\mathrm{d}t}\left(\frac{\partial \mathcal{L}}{\partial \dot{q}_l}\right) - \frac{\partial \mathcal{L}}{\partial q_l} - Q_{q_l} = 0 \tag{1.4}$$

where q_l are the generalized coordinates we choose, Q_{q_l} are the external generalized forces.

We can simplify the Lagrange equations to get equations of motion to describe the behavior of a physical system in terms of its motion as a function of time. With appropriate initial conditions and configurations, we can simulate this dynamic system by those equations.

1.3.2 Linear System

A linear system is a mathematical model of a system based on the use of a linear operator. Linear systems typically exhibit features and properties that are much simpler than the nonlinear case. A continuous-time state-space linear system is defined by the following two equations[8]:

$$\begin{aligned} \dot{x}(t) &= A(t)x(t) + B(t)u(t), \quad u \in \mathbb{R}^k, x \in \mathbb{R}^n \\ y(t) &= C(t)x(t) + D(t)u(t), \quad y \in \mathbb{R}^m \end{aligned} \tag{1.5}$$

The signal

$$u : [0, \infty) \to \mathbb{R}^k, x : [0, \infty) \to \mathbb{R}^n, y : [0, \infty) \to \mathbb{R}^m \tag{1.6}$$

are called the input, state, and output of the system respectively. Equations (1.5) express an input-output relationship between the input signal $u(\cdot)$ and the output signal $y(\cdot)$. For

a given input $u(\cdot)$, we need to solve the state equation to determine the state $x(\cdot)$ and then replace it in the output equation to obtain the output $y(\cdot)$.

A discrete-time state-space linear system is defined by the following two equations:

$$\begin{aligned} x(t+1) &= A(t)x(t) + B(t)u(t), \quad u \in \mathbb{R}^k, x \in \mathbb{R}^n \\ y(t) &= C(t)x(t) + D(t)u(t), \quad y \in \mathbb{R}^m \end{aligned} \tag{1.7}$$

All the terminology introduced for continuous-time systems also applies to discrete time, except that now the domain of the signals is $N := \{0, 1, 2, \cdots\}$, instead of the interval $[0, \infty)$.

In discrete-time systems, the state equation is a difference equation, instead of a first-order differential equation. However, the input-output relationship between input and output is analogous. For a given input $u(\cdot)$, we need to solve the state (difference) equation to determine the state $x(\cdot)$ and then replace it in the output equation to obtain the output $y(\cdot)$.

1.3.3 The Moore-Penrose Pseudoinverse

A the Moore-Penrose pseudoinverse, A^+, of a matrix A is a generalization of the inverse matrix that can be computed for a matrix A that is not necessarily full rank nor square. It can be computed using the singular value decomposition. If matrix A is square, nonsingular, the inverse A^{-1} of matrix A is the same as the pseudoinverse A^+ [9].

Definition 1.3.4. *The pseudoinverse A^+ of a matrix A satisfies all of the following four criteria:*

$$\begin{aligned} &1. AA^+A = A \\ &2. A^+AA^+ = A^+ \\ &3. \left(AA^+\right)^* = AA^+ \\ &4. \left(A^+A\right)^* = A^+A \end{aligned} \tag{1.8}$$

Given the equation $Ax = b$, with $x \in \mathbb{R}^n, b \in \mathbb{R}^m, A \in \mathbb{R}^{n \times m}$, it may not have a solution or an unique solution in general. In that case $x = A^+b$ is the vector that minimizes $\|Ax - b\|_2$.

Chapter 2

Discrete Dynamic Model

2.1 Force Controlled System

We propose an approximate discrete model. The cable is represented by n rigid cylindrical segments connected to each other by spherical joints. One end of the cable is attached to a fixed base, while the other end is controlled.

In this section, we assume that external input quantities are the forces applied at the free end of the cable, respectively donated by $\begin{bmatrix} f_x \\ f_y \\ f_z \end{bmatrix}$. This system has $2n$ degrees of freedom. As shown in Figure 2.1, We choose the generalized coordinates as the angles made by each of n segments with the positive X axis in the XY-plane, $\theta_i, i = 1, 2, \cdots, n$, and the angles made by each of the n segments with the positive Z axis, $\phi_i, i = 1, 2, \cdots, n$, all with respect to a global inertial frame of reference.

Assuming that one end of the cable is fixed at $\begin{bmatrix} 0 \\ 0 \\ 0 \end{bmatrix}$, the position of the center of mass

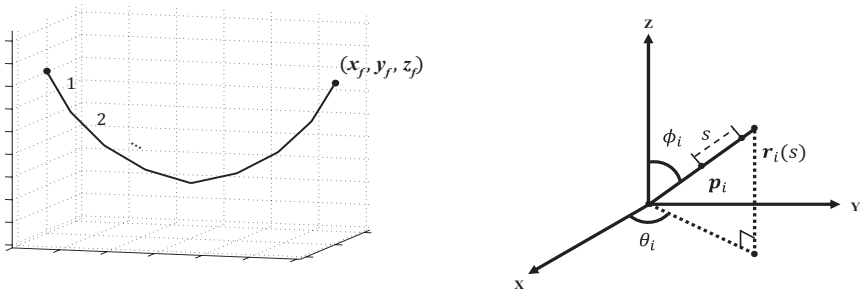

(a) A discrete dynamic model consisting of n rigid segments.

(b) The i^{th} segment.

Figure 2.1: A discrete dynamic model.

of the i^{th} segment is given by,

$$\boldsymbol{p}_i = \sum_{j=1}^{i-1} L_j \begin{bmatrix} \cos(\theta_j) \cdot \sin(\phi_j) \\ \sin(\theta_j) \cdot \sin(\phi_j) \\ \cos(\phi_j) \end{bmatrix} + \frac{L_i}{2} \begin{bmatrix} \cos(\theta_i) \cdot \sin(\phi_i) \\ \sin(\theta_i) \cdot \sin(\phi_i) \\ \cos(\phi_i) \end{bmatrix} \tag{2.1}$$

where L_i is the length of the i^{th} segment.

Thus the velocity of the center of mass of the i^{th} segment is given by,

$$\boldsymbol{v}_i = \dot{\boldsymbol{p}}_i = \frac{\mathrm{d}\boldsymbol{p}_i}{\mathrm{d}t} \tag{2.2}$$

The velocity of a point, $\boldsymbol{r}_i(s)$, at a distance s from its center, $\boldsymbol{p}_i(s)$, (Figure 2.1(b)) is given by,

$$\dot{\boldsymbol{r}}_i(s) = \frac{\mathrm{d}}{\mathrm{d}t} \left(\boldsymbol{p}_i + s \begin{bmatrix} \cos(\theta_j) \cdot \sin(\phi_j) \\ \sin(\theta_j) \cdot \sin(\phi_j) \\ \cos(\phi_j) \end{bmatrix} \right) \tag{2.3}$$

If we consider the drag force, the net external force and torque due to drag on the i^{th}

segment is thus given by,

$$\begin{aligned} \boldsymbol{F}_i = \begin{bmatrix} F_{i,x} \\ F_{i,y} \\ F_{i,z} \end{bmatrix} &= -\int_{-\frac{L_i}{2}}^{\frac{L_i}{2}} C_d \cdot \dot{\boldsymbol{r}}_i(s) ds \\ \tau_i &= -\int_{-\frac{L_i}{2}}^{\frac{L_i}{2}} \dot{\boldsymbol{r}}_i(s) \times (C_d \cdot \dot{\boldsymbol{r}}_i(s))\, ds \end{aligned} \tag{2.4}$$

where C_d is an coefficient of the frag force. We assume $C_d = 0.003$.

The angular velocity of the i^{th} segment is given by,

$$\boldsymbol{\omega}_i = \dot{\theta}_i \begin{bmatrix} 0 \\ 0 \\ 1 \end{bmatrix} + \dot{\phi}_i \begin{bmatrix} -\sin(\theta_i) \\ \cos(\theta_i) \\ 0 \end{bmatrix} \tag{2.5}$$

We can define the *free* end of the cable in terms of the generalized coordinates as,

$$\begin{bmatrix} x_f \\ y_f \\ z_f \end{bmatrix} = \sum_{i=1}^{n} L_i \begin{bmatrix} \cos(\theta_i) \cdot \sin(\phi_i) \\ \sin(\theta_i) \cdot \sin(\phi_i) \\ \cos(\phi_i) \end{bmatrix} \tag{2.6}$$

Thus, we can define the $2n$ generalized forces,

$$
\begin{aligned}
Q_{\theta_i} &= \begin{bmatrix} f_x \\ f_y \\ f_z \end{bmatrix} \cdot \frac{\partial \begin{bmatrix} x_f \\ y_f \\ z_f \end{bmatrix}}{\partial \theta_i} + \sum_{j=1}^{n} \boldsymbol{F}_i \cdot \frac{\partial \boldsymbol{p}_j}{\partial \theta_i} + \sum_{j=1}^{n} \tau_i \cdot \frac{\partial \boldsymbol{\omega}_j}{\partial \dot{\theta}_i} \\
&= -f_x L_i \sin(\theta_i) \sin(\phi_i) + f_y L_i \cos(\theta_i) \sin(\phi_i) \\
&\quad + \sum_{j=1}^{n} \boldsymbol{F}_i \cdot \frac{\partial \boldsymbol{p}_j}{\partial \theta_i} + \sum_{j=1}^{n} \tau_i \cdot \frac{\partial \boldsymbol{\omega}_j}{\partial \dot{\theta}_i} \\
Q_{\phi_i} &= \begin{bmatrix} f_x \\ f_y \\ f_z \end{bmatrix} \cdot \frac{\partial \begin{bmatrix} x_f \\ y_f \\ z_f \end{bmatrix}}{\partial \phi_i} + \sum_{j=1}^{n} \boldsymbol{F}_i \cdot \frac{\partial \boldsymbol{p}_j}{\partial \phi_i} + \sum_{j=1}^{n} \tau_i \cdot \frac{\partial \boldsymbol{\omega}_j}{\partial \dot{\phi}_i} \\
&= f_x L_i \cos(\theta_i) \cos(\phi_i) + f_y L_i \sin(\theta_i) \cos(\phi_i) \\
&\quad - f_z L_i \sin(\phi_i) + \sum_{j=1}^{n} \boldsymbol{F}_i \cdot \frac{\partial \boldsymbol{p}_j}{\partial \phi_i} + \sum_{j=1}^{n} \tau_i \cdot \frac{\partial \boldsymbol{\omega}_j}{\partial \dot{\phi}_i} \\
&\quad \forall i = 1, 2, \cdots, n
\end{aligned}
\tag{2.7}
$$

where m_i is the mass of the i^{th} segment, g is the gravitational acceleration, $\hat{\boldsymbol{k}}$ is $\begin{bmatrix} 0 \\ 0 \\ 1 \end{bmatrix}$.

The Kinetic Energy of the system is given by,

$$
K = \sum_{i=1}^{n} \left(\frac{1}{2} m_i |\dot{\boldsymbol{p}}_i|^2 + \frac{1}{2} \frac{m_i {L_i}^2}{12} |\boldsymbol{\omega}_i|^2 \right) \tag{2.8}
$$

The Potential Energy is given by,

$$
V = \sum_{i=1}^{n} m_i g \hat{\boldsymbol{k}} \cdot \boldsymbol{p}_i \tag{2.9}
$$

Thus, Lagrangian is given by,

$$\mathcal{L} = K - V \tag{2.10}$$

The Lagrange equations of motion for the system is given by,

$$\begin{aligned} &\frac{\mathrm{d}}{\mathrm{d}t}\left(\frac{\partial \mathcal{L}}{\partial \dot{q}_l}\right) - \frac{\partial \mathcal{L}}{\partial q_l} - Q_{q_l} = 0 \\ &\qquad \forall q_l \in \{\theta_1, \theta_2, \cdots, \theta_n, \phi_1, \phi_2, \cdots, \phi_n\} \end{aligned} \tag{2.11}$$

The equations (2.11) consist of $2n$ second order ordinary differential equations in the quantities $\{\theta_1, \theta_2, \cdots, \theta_n, \phi_1, \phi_2, \cdots, \phi_n\}$. Moreover they are affine in $\left\{\ddot{\theta_1}, \ddot{\theta_2}, \cdots, \ddot{\theta_n}, \ddot{\phi_1}, \ddot{\phi_2}, \cdots, \ddot{\phi_n}\right\}$. Thus for a given initial values of $\{\theta_1, \theta_2, \cdots, \theta_n, \phi_1, \phi_2, \cdots, \phi_n\}$ and $\left\{\dot{\theta_1}, \dot{\theta_2}, \cdots, \dot{\theta_n}, \dot{\phi_1}, \dot{\phi_2}, \cdots, \dot{\phi_n}\right\}$ at $t = 0$, and given the external force profiles, $\{f_x, f_y, f_z\}$ as function of t, we can numerically integrate these equations to obtain the complete dynamics of the system.

2.2 Position Controlled System

In this section, we need to slightly re-formulate the equations of motion, (2.11). In position controlled system, $\{f_x, f_y, f_z\}$ are unknown and $\{x_f, y_f, z_f\}$ are the specified variables.

Thus, we still need $2n$ generalized coordinates, $\{\theta_1, \theta_2, \cdots, \theta_n, \phi_1, \phi_2, \cdots, \phi_n\}$. Equations and the expression for the generalized forces, (2.7), kinetic energy, (2.8), and potential energy, (2.9), still remain the same. We still have $2n$ Lagrange equations of motion. However now we have $2n + 3$ unknown.

Taking time derivative of the configuration constraint equations, (2.6), we obtain the

velocity constraint equations,

$$\begin{bmatrix} \dot{x_f} \\ \dot{y_f} \\ \dot{z_f} \end{bmatrix} - \sum_{i=1}^{n} L_i \Bigg(\dot{\theta}_i \begin{bmatrix} -\sin(\theta_i) \cdot \sin(\phi_i) \\ \cos(\theta_i) \cdot \sin(\phi_i) \\ 0 \end{bmatrix} + \dot{\phi}_i \begin{bmatrix} \cos(\theta_i) \cdot \cos(\phi_i) \\ \sin(\theta_i) \cdot \cos(\phi_i) \\ -\sin(\phi_i) \end{bmatrix} \Bigg) = 0 \tag{2.12}$$

And we differentiating it for a second time we obtain the acceleration constraint equations,

$$\begin{bmatrix} \ddot{x_f} \\ \ddot{y_f} \\ \ddot{z_f} \end{bmatrix} - \sum_{i=1}^{n} L_i \Bigg(\dot{\theta}_i^2 \begin{bmatrix} -\cos(\theta_i) \cdot \sin(\phi_i) \\ -\sin(\theta_i) \cdot \sin(\phi_i) \\ 0 \end{bmatrix} + \dot{\phi}_i^2 \begin{bmatrix} -\cos(\theta_i) \cdot \sin(\phi_i) \\ -\sin(\theta_i) \cdot \sin(\phi_i) \\ -\cos(\phi_i) \end{bmatrix} + \dot{\theta}_i \dot{\phi}_i \begin{bmatrix} -2\sin(\theta_i) \cdot \cos(\phi_i) \\ 2\cos(\theta_i) \cdot \cos(\phi_i) \\ 0 \end{bmatrix} + \ddot{\theta}_i \begin{bmatrix} -\sin(\theta_i) \cdot \sin(\phi_i) \\ \cos(\theta_i) \cdot \sin(\phi_i) \\ 0 \end{bmatrix} + \ddot{\phi}_i \begin{bmatrix} \cos(\theta_i) \cdot \cos(\phi_i) \\ \sin(\theta_i) \cdot \cos(\phi_i) \\ -\sin(\phi_i) \end{bmatrix} \Bigg) = 0 \tag{2.13}$$

Equations (2.11) and (2.13) together form $2n+3$ equations, which are corresponding to $2n+3$ unknowns, $\left\{ f_x, f_y, f_z, \ddot{\theta_1}, \ddot{\theta_2}, \cdots, \ddot{\theta_n}, \ddot{\phi_1}, \ddot{\phi_2}, \cdots, \ddot{\phi_n} \right\}$. Thus, for given trajectories of the free end of the cable (*i.e.* given $\{x_f, y_f, z_f\}$ and their derivatives as a function of time), and an initial configuration $\{\theta_1, \theta_2, \cdots, \theta_n, \phi_1, \phi_2, \cdots, \phi_n\}$ that satisfy the shape constraint equations, and an initial set of angular velocities $\left\{ \dot{\theta_1}, \dot{\theta_2}, \cdots, \dot{\theta_n}, \dot{\phi_1}, \dot{\phi_2}, \cdots, \dot{\phi_n} \right\}$ that satisfy the velocity constraint equations at $t = 0$, we can integrate and solve the Equations (2.11) and (2.13) for $\{f_x, f_y, f_z, \theta_1, \theta_2, \cdots, \theta_n, \phi_1, \phi_2, \cdots, \phi_n\}$.

2.3 Simulations and Results

2.3.1 Force Controlled System

For simulating the system, we used Mathematica to simplify the Equations (2.11) to obtain the ODEs and the coefficients of the second derivatives in the equations. The equations were numerically integrated by MATLAB. Figure 2.2(a)- 2.2(d) shows an example of the force controlled system simulation.

2.3.2 Position Controlled System

For simulating the system, we used Mathematica to simplify the Equations (2.11) and (2.13) to obtain the ODEs and the coefficients of the second derivatives in the equations. The equations were numerically integrated by MATLAB. Figure 2.3(a)- 2.3(b) shows an example of the position controlled system simulation.

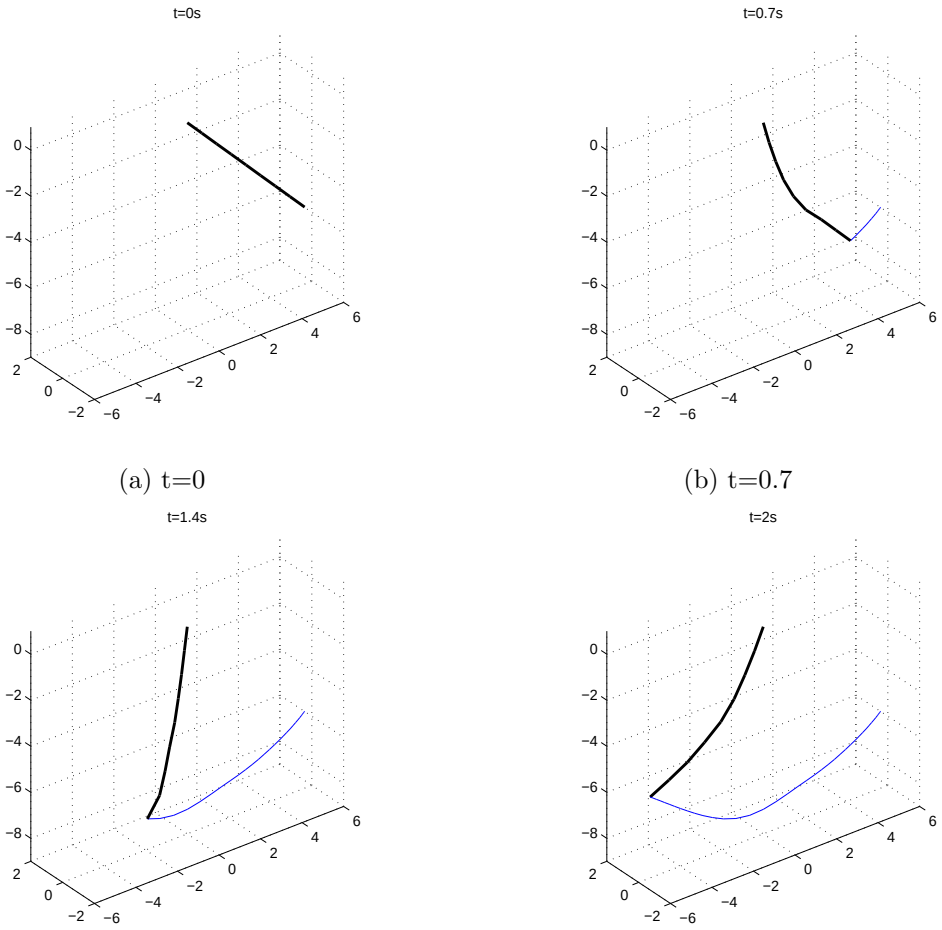

(a) t=0 (b) t=0.7

(c) t=1.4 (d) t=2

Figure 2.2: Traces of complete dynamic simulations of a cable showing screenshots from a force controlled simulation and demonstrates a swing due to gravity (8-segment system).

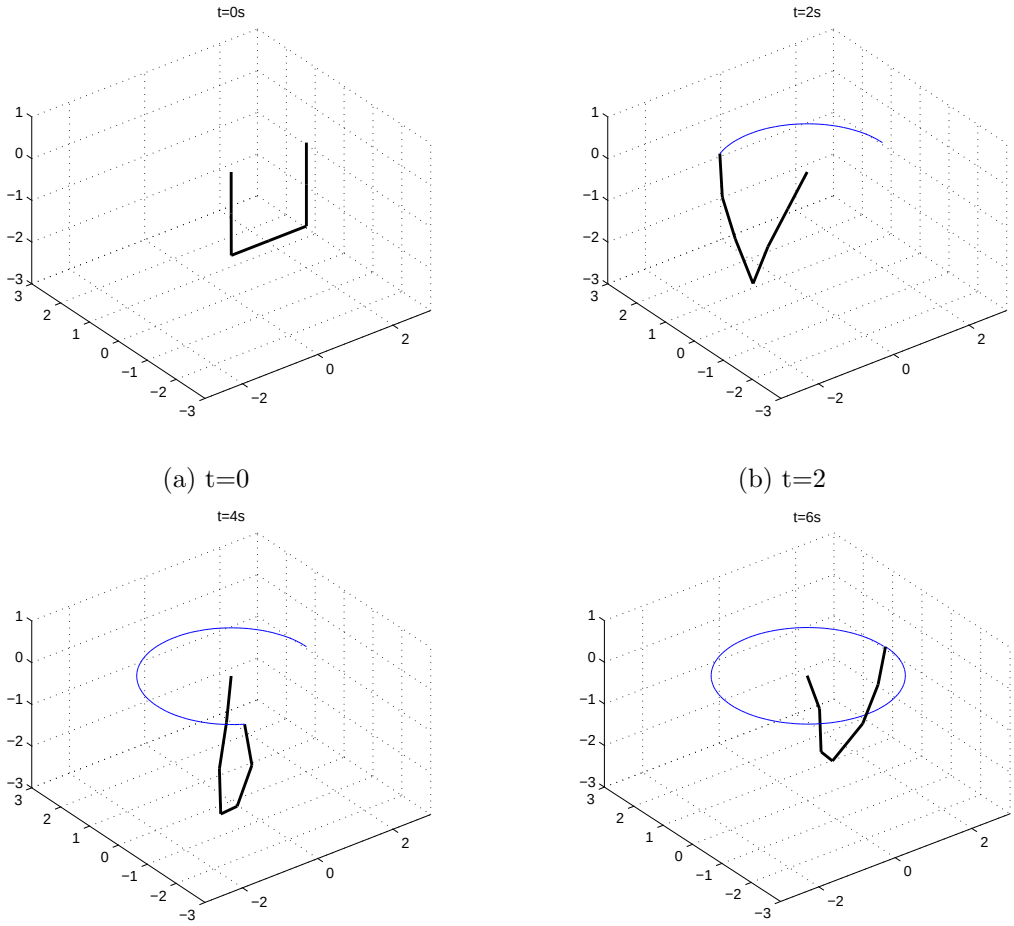

(a) t=0

(b) t=2

(c) t=4

(d) t=6

Figure 2.3: Traces of complete dynamic simulations of a cable showing screenshots from a position controlled simulation and demonstrates a circular motion of the free end (6-segment system).

Chapter 3

Shape Control of the Cable

3.1 The Design of Controller

The governing equations of the system is given by Equations (2.11). We have a total of $2n$ equations. These equations involve the $2n+3$ variables, $\{f_x, f_y, f_z, \theta_1, \theta_2, \cdots, \theta_n, \phi_1, \phi_2, \cdots, \phi_n\}$, and their derivatives. The governing equations can be written as

$$M_{2n\times 2n}\begin{bmatrix}\ddot{\Theta}\\ \ddot{\Phi}\end{bmatrix} + N_{2n\times 1}\left(\Theta, \Phi, \dot{\Theta}, \dot{\Phi}\right) + Q_{2n\times 3}\left(\Theta, \Phi\right)\begin{bmatrix}f_x\\ f_y\\ f_z\end{bmatrix} = 0 \tag{3.1}$$

where, $\Theta = [\theta_1, \theta_2, \cdots, \theta_n]^{\mathrm{T}}$, $\Phi = [\phi_1, \phi_2, \cdots, \phi_n]^{\mathrm{T}}$, $\dot{\Theta} = [\dot{\theta}_1, \dot{\theta}_2, \cdots, \dot{\theta}_n]^{\mathrm{T}}$, $\dot{\Phi} = [\dot{\phi}_1, \dot{\phi}_2, \cdots, \dot{\phi}_n]^{\mathrm{T}}$, $\ddot{\Theta} = [\ddot{\theta}_1, \ddot{\theta}_2, \cdots, \ddot{\theta}_n]^{\mathrm{T}}$, $\ddot{\Phi} = [\ddot{\phi}_1, \ddot{\phi}_2, \cdots, \ddot{\phi}_n]^{\mathrm{T}}$, N is a function of Θ, Φ, $\dot{\Theta}$, $\dot{\Phi}$, Q is a function of Θ, Φ.

We can substitute $\dot{\Theta}$ into p, $\dot{\Phi}$ into q such that $\ddot{\Theta} = \dot{p}$, $\ddot{\Phi} = \dot{q}$. Thus the governing equations can be written as

$$M\begin{bmatrix}\dot{p}\\ \dot{q}\end{bmatrix} + N + Q\begin{bmatrix}f_x\\ f_y\\ f_z\end{bmatrix} = 0 \tag{3.2}$$

We propose the control law

$$\begin{bmatrix} f_x \\ f_y \\ f_z \end{bmatrix} = -Q^{+}\left(M \begin{bmatrix} \dot{p} \\ \dot{q} \end{bmatrix} + N \right) \tag{3.3}$$

where, $(\cdot)^{+}$ is the Moore-Penrose pseudoinverse.

Denote the desired shape of the discrete model by $\Theta^D = [\theta_1^D, \theta_2^D, \cdots, \theta_n^D]^{\mathrm{T}}$ and $\Phi^D = [\phi_1^D, \phi_2^D, \cdots, \phi_n^D]^{\mathrm{T}}$. Then we assume that

$$\begin{bmatrix} p^D \\ q^D \end{bmatrix} = \begin{bmatrix} \dot{\Theta} \\ \dot{\Phi} \end{bmatrix} = K_1 \left(\begin{bmatrix} \Theta^D \\ \Phi^D \end{bmatrix} - \begin{bmatrix} \Theta \\ \Phi \end{bmatrix} \right) \tag{3.4}$$

$$\begin{bmatrix} \dot{p} \\ \dot{q} \end{bmatrix} = K_2 \left(\begin{bmatrix} p^D \\ q^D \end{bmatrix} - \begin{bmatrix} p \\ q \end{bmatrix} \right) \tag{3.5}$$

where, K_1 and K_2 are $n \times n$ gain matrices.

Then the control law can be written as

$$\begin{aligned} \begin{bmatrix} f_x \\ f_y \\ f_z \end{bmatrix} &= -Q^{+}\left[MK_2 \left(\begin{bmatrix} p^D \\ q^D \end{bmatrix} - \begin{bmatrix} p \\ q \end{bmatrix} \right) + N \right] \\ &= -Q^{+}\left\{ MK_2 \left[K_1 \left(\begin{bmatrix} \Theta^D \\ \Phi^D \end{bmatrix} - \begin{bmatrix} \Theta \\ \Phi \end{bmatrix} \right) - \begin{bmatrix} p \\ q \end{bmatrix} \right] + N \right\} \end{aligned} \tag{3.6}$$

Thus for a given desired shape of the discrete model, an initial configuration that satisfy the shape constraint equations and an initial set of angular velocity that satisfy the velocity constraint equations, we can solve Equations (3.6) for $\{f_x, f_y, f_z\}$. Though we do not have full controllability of the system, with $\{f_x, f_y, f_z\}$ we can use the force controlled system to control the shape of cable and achieve an approximation of the desired shape.

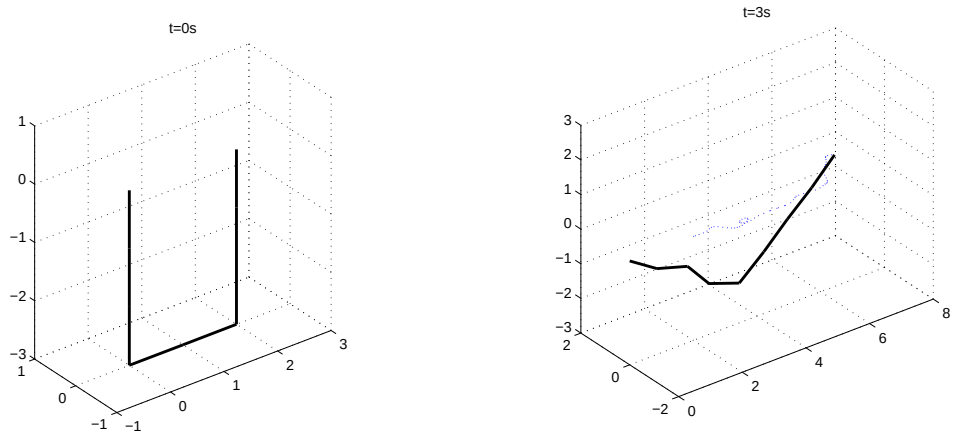

(a) Initial shape.

(b) Final shape attained is approximately a straight line.

Figure 3.1: Shape control example: Desired shape is a straight line.

3.2 Simulation Results of Shape Control

3.2.1 Simulations With Gravity and Without Darg Force

Figure 3.1 shows an attempt to control the shape of a 8-segment model, where the desired shape is a straight line. As shown in Figure 3.1(b), the controller was able to achieve an approximation of the desired shape.

Figure 3.2 shows an attempt to control the end of a 8-segment cable model doing a circular motion. The desired shape is a function of time. As shown in Figure 3.2(b), the controller was able to do a approximation of the desired motion.

3.2.2 Simulations Without Gravity and Drag Force

In some occasions, the control forces applied on the end of the cable are much greater than gravity. Then the control forces are dominant during the simulation. In order to simplify the simulation, we can ignore the gravity during the simulation when control forces dominant over gravity. Under this condition, the gravity acceleration is simplified to

$$g = 0 \tag{3.7}$$

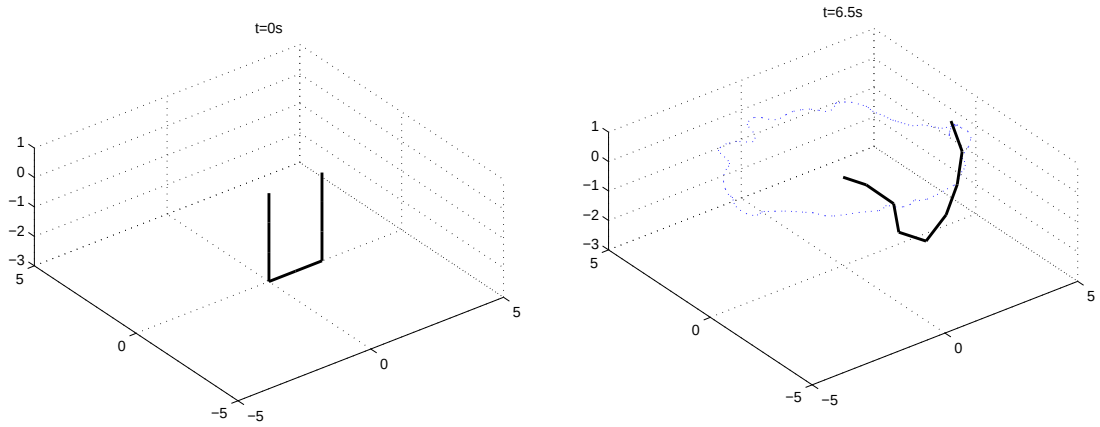

(a) Initial shape.

(b) The trajectories of the end of the cable is approximately a circle.

Figure 3.2: Shape control example: Desired shape is a function of time (The end of the cable moving in circular motion).

For example, if we want to reverse an arch from opening up to opening down, we expect to exert a tremendous force upward then downward at the end of the cable in a short time. In this case, the control force at the end of the cable is much greater than gravity and dominant over gravity. Therefore, simulating this case without gravity is reasonable. Figure 3.3 shows the initial shape and desired shape for this case (8-segment). The desired shape used is $\Theta^D = [0, 0, 0, 0, 0, 0, 0, 0]^{\mathrm{T}}$ and $\Phi^D = [0.52, 0.79, 1.05, 1.31, 1.83, 2.10, 2.36, 2.62]^{\mathrm{T}}$ and gain matrix used is $K = 0.7I$.

Figure 3.4 shows the simulation result by MATLAB. We note that when $t = 2.95s$ the shape of the cable approximated the arch which is opening down.

We define the error of the simulation is

$$Error = \frac{\sum_{i=1}^{n} \left(\theta_i^C - \theta_i^D\right)^2 + \sum_{i=1}^{n} \left(\phi_i^C - \phi_i^D\right)^2}{2n} \tag{3.8}$$

where n is the number of segments, θ_i^C and ϕ_i^C are current angles during the simulation, θ_i^D and ϕ_i^D are the desired angles.

Figure 3.5 shows the graphs of forces and error of the simulation. From the force graph (Figure 3.5(a)), we note that the control force was upward in a sudden at the beginning

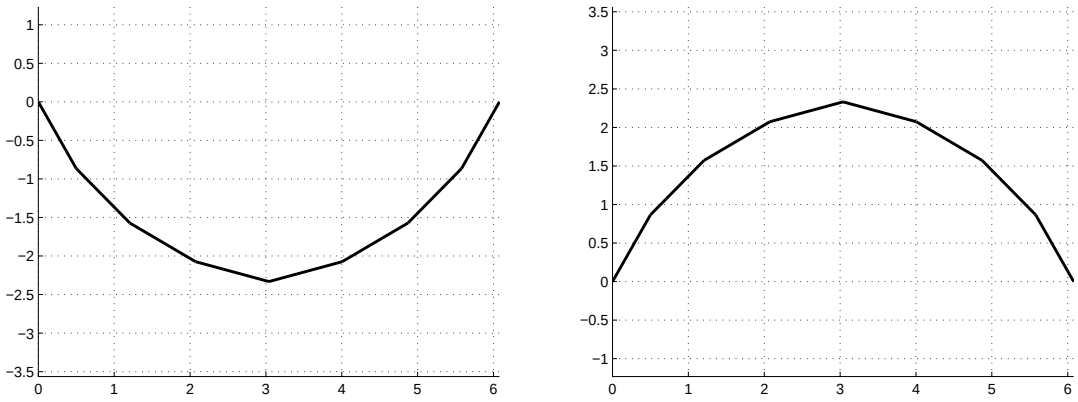

(a) Initial shape.

(b) Disired shape.

Figure 3.3: Shape control example: Initial shape and desired shape for reversing an arch (8-segment).

and then went downward in a short time. This result is in line with our expectation. From the error graph (Figure 3.5(b)), we note that the error decreased over time until $t = 3s$ and when $t = 3s$ the error was nearly smallest which means the shape of the cable approximated the desired shape best. When $t > 3s$, the error increases because of the inertia.

According to the simulation result above, the controller was able to achieve a satisfactory approximation of the desired shape in this case. However, our control law is based on the Moore-Penrose pseudoinverse and definitely not guaranteed to achieve the desired shape exactly no matter what n is. Nevertheless, we note that the smaller the number of segments is, the more accurate the simulation will be. We can have a better simulation result if we use smaller number of segments n.

Figure 3.6 shows the initial shape and desired shape for the 3-segment system. The desired shape used is $\Theta^D = [0, 0, 0]^{\mathrm{T}}$ and $\Phi^D = [0.79, 1.57, 2.36]^{\mathrm{T}}$ and gain matrix used is $K = 0.6I$.

Figure 3.7 shows the simulation result by MATLAB. We note that when $t = 3.95s$ the shape of the cable was nearly the same as the desired shape. Apparently, the simulation result of 3-segment system is much better than the result of 8-segment system.

Figure 3.8 shows the graphs of forces and error of the simulation of the 3-segment system.

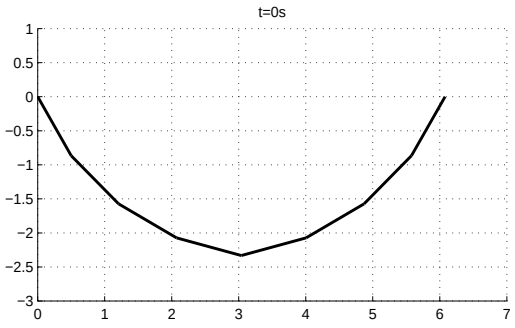

(a) t = 0s.

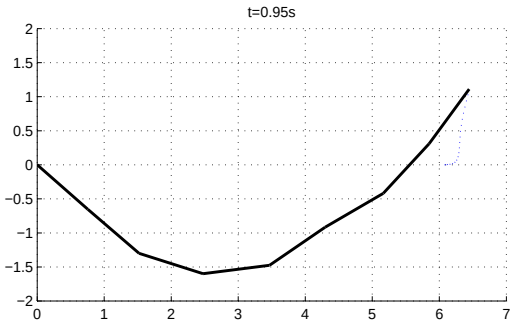

(b) t = 0.95s.

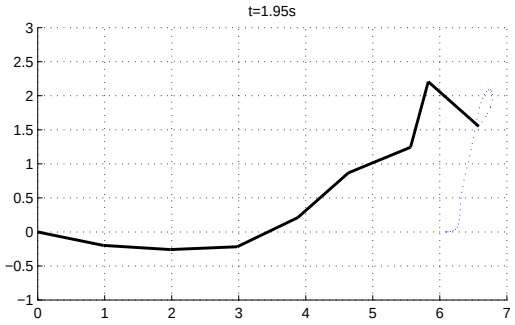

(c) t = 1.95s.

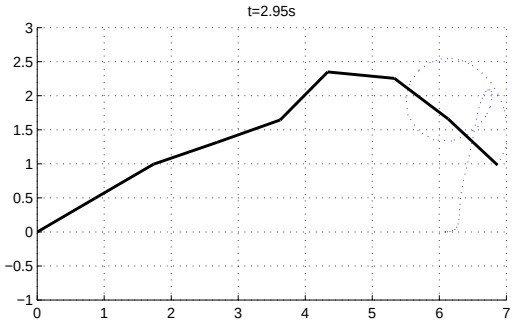

(d) t = 2.95s.

Figure 3.4: Shape control example: Simulations for reversing an arch (8-segment).

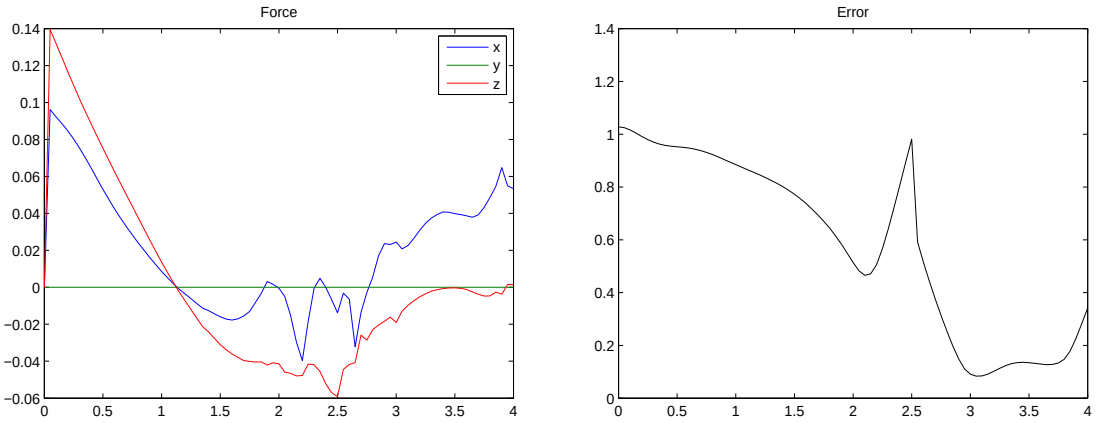

(a) Forces. (b) Error.

Figure 3.5: Shape control example: The graphs of forces and error for the simulation of reversing an arch (8-segment).

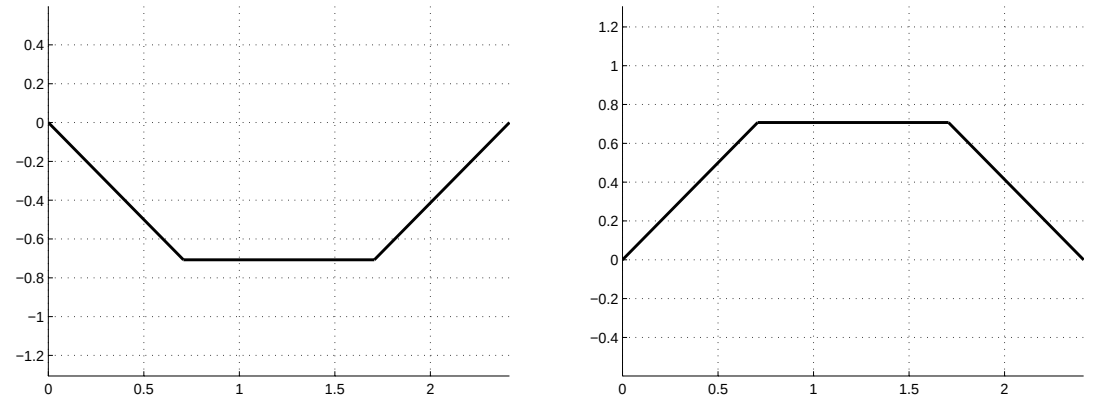

(a) Initial shape. (b) Disired shape.

Figure 3.6: Shape control example: Initial shape and desired shape for reversing an arch (3-segment).

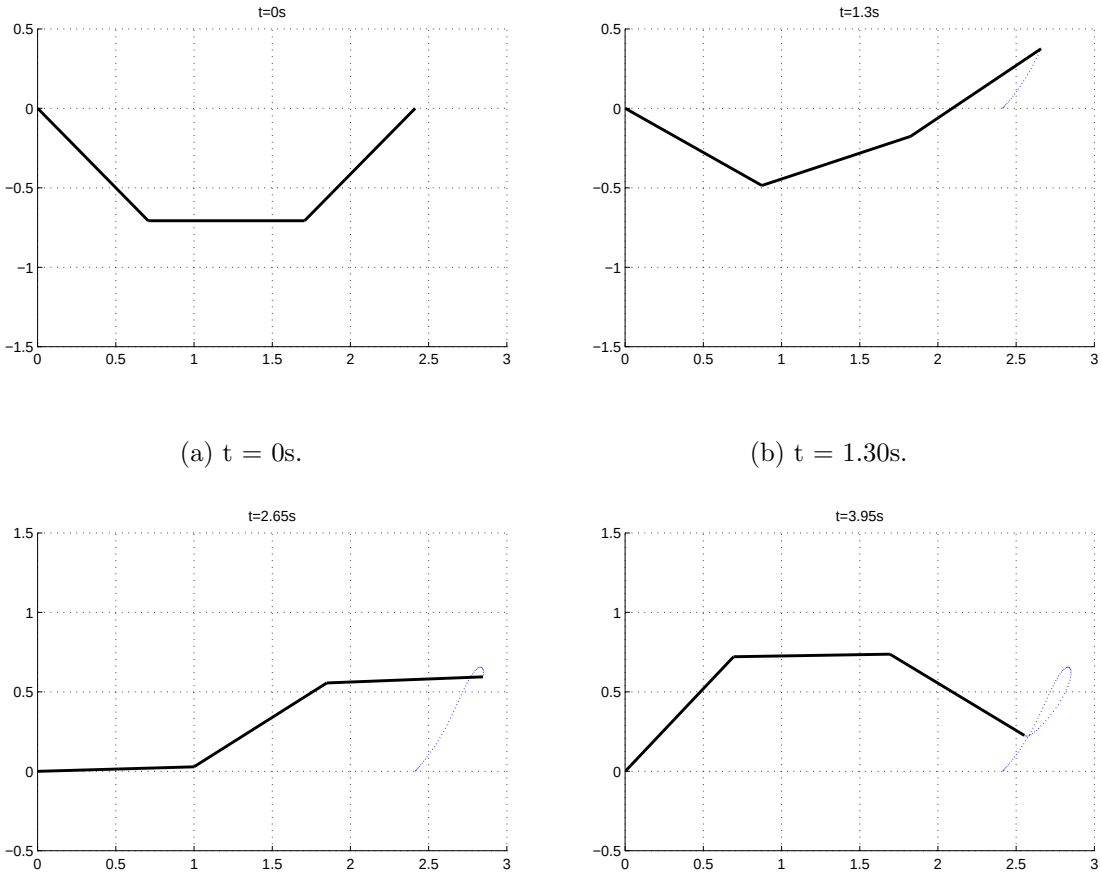

(a) t = 0s.

(b) t = 1.30s.

(c) t = 2.65s.

(d) t = 3.95s.

Figure 3.7: Shape control example: Simulations for reversing an arch (3-segment).

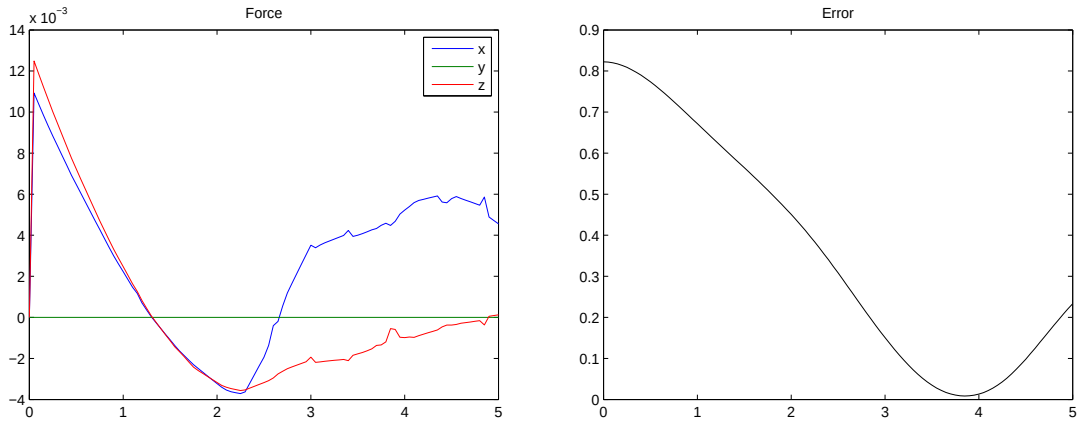

(a) Forces. (b) Error.

Figure 3.8: Shape control example: The graphs of forces and error for the simulation of reversing an arch (3-segment).

The force graph (Figure 3.8(a)) of 3-segment system is consistent with the forces graph of 8-segment system (Figure 3.5(a)). From the error graph (Figure 3.8(b)), we note that the error was minimum when t approximately equals to $3.9s$. The minimum error of 3-segment system is much smaller than the minimum error of 8-segment system. It proved that the smaller number of segments will lead a better approximation of the desired shape, which means it is easier to control with a smaller n.

Though the shape of the cable can be controlled to attain the desired shape at an instant, it cannot keep the desired shape for a long time due to inertia and gravity. Consequently, the controller should be capable to correct to the desired shape continuously.

Figure 3.9 shows the simulation result of 3-segment system for a longer time. Though the shape of the cable started to deviate the desired shape after $t = 3s$, the controller managed to achieve the desired shape again when $t = 20s$ and $t = 33.5s$ (Figure 3.9(a) and Figure 3.9(b)). Also from the error graph (Figure 3.9(c)), we can see that the error increased and decreased periodically, which means the shape of cable achieved and deviated the desired shape periodically. The controller kept trying to correct the shape of the cable to the desired shape. According to the simulation result, this controller has the capability to control the shape of the cable continuously.

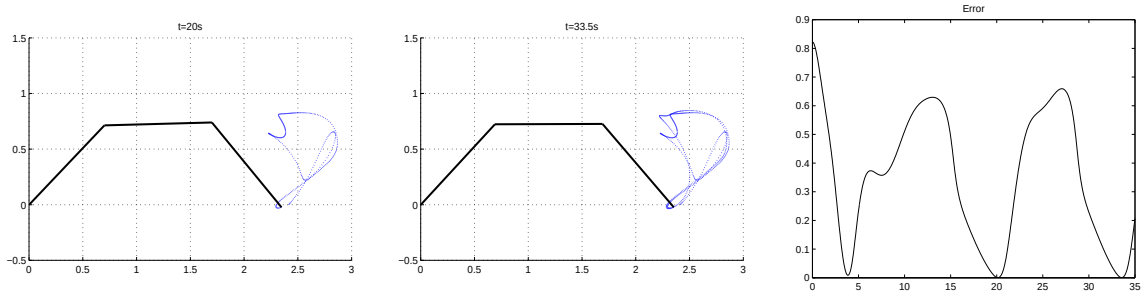

(a) t=20s. (b) t=33.5s. (c) Error.

Figure 3.9: The simulation of reversing an arch (3-segment) for a longer time (only the best matches with the desired shape shown).

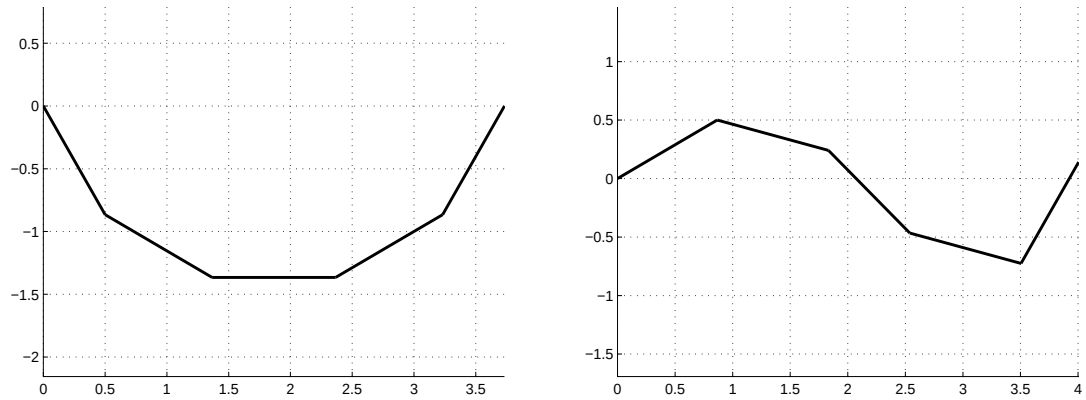

(a) Initial shape. (b) Disired shape.

Figure 3.10: Shape control example with drag force: Initial shape and desired shape (5-segment).

3.2.3 Simulations With Drag Force and Without Gravity

In some conditions, the cable moves in a high speed and the air resistance plays a significant role during the simulations. If we still ignore the drag force, the cable may lose control and can never be controlled back to the desired shape. In this condition, we need to consider the drag force. Figure 3.10 below shows the initial shape and desired shape for this case (5-segment).

Figure 3.11 shows the simulation result by MATLAB. We note that when $t > 5s$ the shape of the cable approximated the desired shape and then cable moved in a very slow

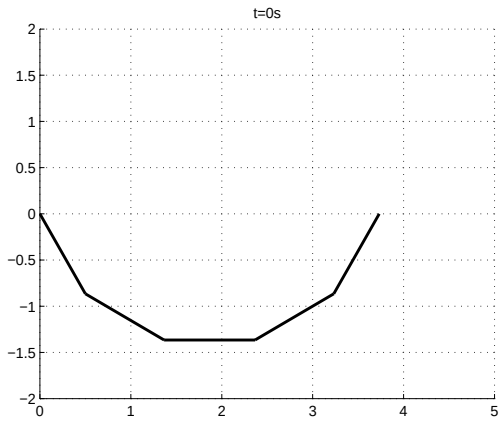

(a) t = 0s.

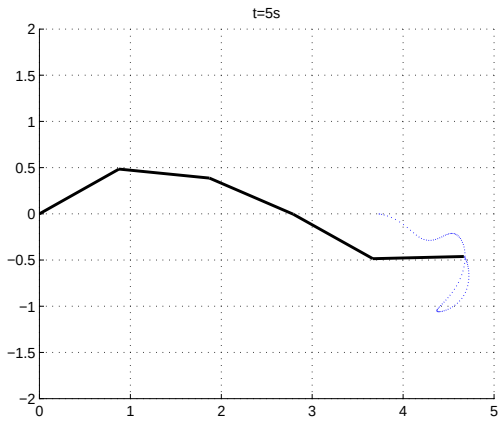

(b) t = 5s.

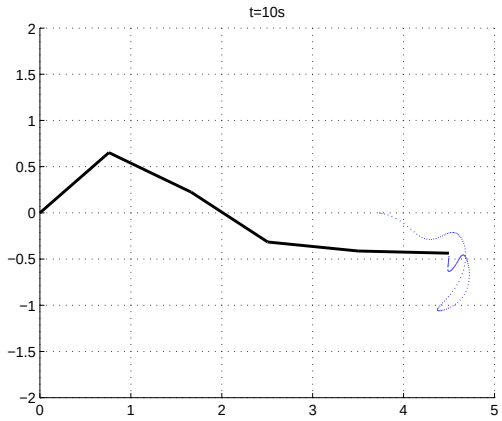

(c) t = 10s.

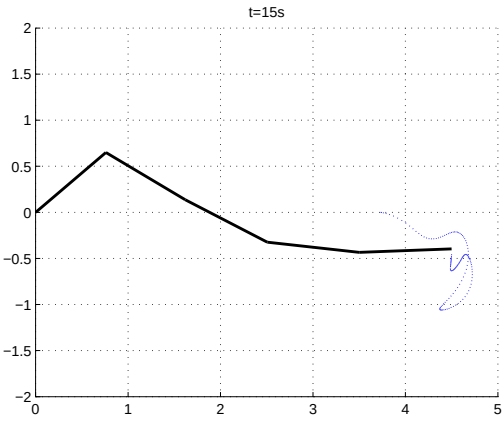

(d) t = 15s.

Figure 3.11: Shape control example: Simulations with drag force (5-segment).

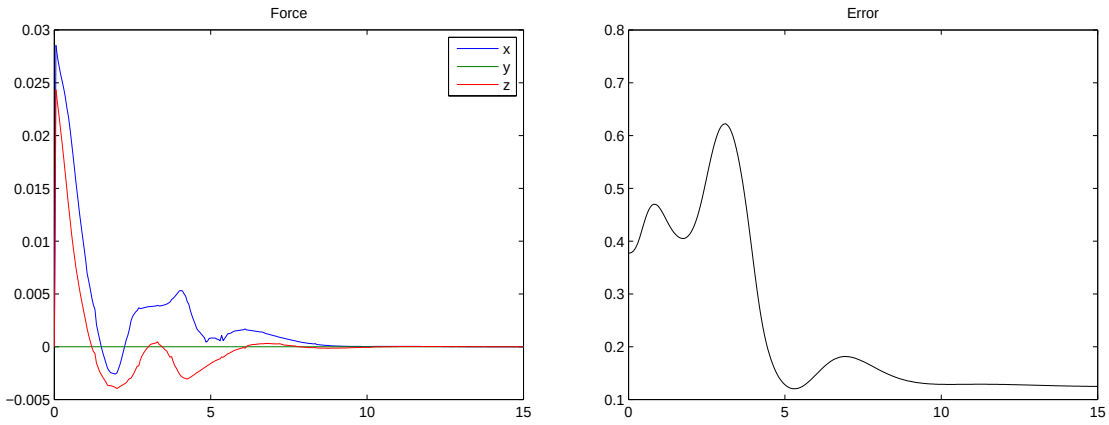

(a) Forces.

(b) Error.

Figure 3.12: Shape control example: The graphs of forces and error for the simulation with drag force (5-segment).

velocity and its shape nearly kept constant due to the drag force.

Figure 3.12 shows the graphs of forces and error of the simulation. From the force graph (Figure 3.12(a)), we note that the control force was very small when $t > 5s$ due to the shape was very close to the desired shape. From the error graph (Figure 3.12(b)), we note that the error decreased rapidly until $t = 5s$ and then the error decreased in a very low rate due to the drag force, which means cable kept deforming to the desired shape in a low rate.

Chapter 4

Stability of the Shape Control Problem

4.1 The Quasi-Static Model

The controller we designed in the last chapter is a linearized controller for a nonlinear system, and hence complicated for long-term stability analysis. Thus, we need to simplify the discrete segment model in order to obtain the state error function. In some occasions, we can ignore the inertial forces if the drag forces dominate over inertial forces. For examples, a slow-moving light cable in spaceship is justified for the quasi-static model because there is no gravity in space and air resistance exists in the spaceship. In addition, a detector connected to a submarine is also a reasonable example if the buoyancy of the detector and cable equals gravity allowing us to ignore the gravity in water. The water resistance dominated over inertial forces for the detector in a very low speed. Under this condition, the equations that govern this system simplify to

$$\begin{aligned} Q_{\theta_i} &= 0 \\ Q_{\phi_i} &= 0 \\ \forall i &= 1, 2, \cdots, n \end{aligned} \tag{4.1}$$

where Q_{θ_i} and Q_{ϕ_i} are given by Equations (2.7).

We note that the external forces, $\boldsymbol{F}_i$, and torques, τ_i are linear in the speeds $\left\{\dot{\theta_1}, \dot{\theta_2}, \cdots, \dot{\theta_n}, \dot{\phi_1}, \dot{\phi_2}, \cdots, \dot{\phi_n}\right\}$. Thus the Q_{θ_i} and Q_{ϕ_i} are linear in $\left\{\dot{\theta_1}, \dot{\theta_2}, \cdots, \dot{\theta_n}, \dot{\phi_1}, \dot{\phi_2}, \cdots, \dot{\phi_n}, f_x, f_y, f_z\right\}$.

Consequently, the equations of the quasi-static model can be written as

$$A_{2n\times 2n}\begin{bmatrix}\dot{\Theta}\\ \dot{\Phi}\end{bmatrix} + B_{2n\times 3}\begin{bmatrix}f_x\\ f_y\\ f_z\end{bmatrix} = 0 \tag{4.2}$$

where $\dot{\Theta} = [\dot{\theta_1}, \dot{\theta_2}, \cdots, \dot{\theta_n}]^{\mathrm{T}}$ and $\dot{\Phi} = [\dot{\phi_1}, \dot{\phi_2}, \cdots, \dot{\phi_n}]^{\mathrm{T}}$.

Then we rewrite the controller for the quasi-static model.

$$\begin{bmatrix}f_x\\ f_y\\ f_z\end{bmatrix} = -B^{+}AK\left(\begin{bmatrix}\Theta^D\\ \Phi^D\end{bmatrix} - \begin{bmatrix}\Theta\\ \Phi\end{bmatrix}\right) \tag{4.3}$$

where $(\cdot)^{+}$ is the Moore-Penrose pseudoinverse and K is an $2n \times 2n$ gain matrix.

Take the force controller back into Equations (4.2), we have

$$A\begin{bmatrix}\dot{\Theta}\\ \dot{\Phi}\end{bmatrix} + B\left[-B^{+}AK\left(\begin{bmatrix}\Theta^D\\ \Phi^D\end{bmatrix} - \begin{bmatrix}\Theta\\ \Phi\end{bmatrix}\right)\right] = 0 \tag{4.4}$$

Define the Error between the current shape of cable and the desired shape of cable as

$$e(t) = \begin{bmatrix}\Theta^D\\ \Phi^D\end{bmatrix} - \begin{bmatrix}\Theta\\ \Phi\end{bmatrix} \tag{4.5}$$

Take time derivatives on both sides of Equation (4.5).

$$\dot{e}(t) = -\begin{bmatrix}\dot{\Theta}\\ \dot{\Phi}\end{bmatrix} \tag{4.6}$$

Take Equations (4.5) and (4.6) back to Equation (4.4).

$$A\left(-\dot{e}(t)\right) + B\left[-B^{+}AKe(t)\right] = 0 \tag{4.7}$$

Then we can write the state error function as

$$\dot{e}(t) = -CKe(t) \tag{4.8}$$

where matrix $C = A^{+}BB^{+}A$.

Note that if all $Re\left\{\lambda_i\left(-CK\right)\right\}$ (i.e. the real parts of the eigenvalues of the matrix $-CK$) are negative, then $e(t)$ tends to be zero as $t \to 0$. However, matrix C is not full rank (the rank of matrix C should be 3 actually). The eigenvalues of matrix C contains zeros. Thus we can only control the system to be marginally stable by setting $Re\left\{\lambda_i\left(-CK\right)\right\}$ non-positive.

If square matrix $C_{2n\times 2n}$ is diagonalizable [10], then matrix C can be factorized as

$$C = U\Lambda U^{-1} \tag{4.9}$$

where U is the square $(2n \times 2n)$ matrix whose i^{th} column is the eigenvector q_i of C and Λ is the diagonal matrix whose diagonal elements are the corresponding eigenvalues. Let $K = U\Lambda^{+}U^{-1}$, where Λ^{+} is the pseudoinverse of matrix Λ. Then

$$CK = U\Lambda U^{-1}U\Lambda^{+}U^{-1} = U\Lambda\Lambda^{+}U^{-1} \tag{4.10}$$

Note that matrix $\Lambda\Lambda^{+}$ is a diagonal matrix whose diagonal elements are only 0 or 1. Thus $Re\left\{\lambda_i\left(-CK\right)\right\}$ becomes all non-positive (only 0 and 1) and this system is marginally stable. Though the error may not be zero as $t \to 0$. The cable will eventually reach an approximation of the desired shape after enough long time, though it may not reach the exact desired shape.

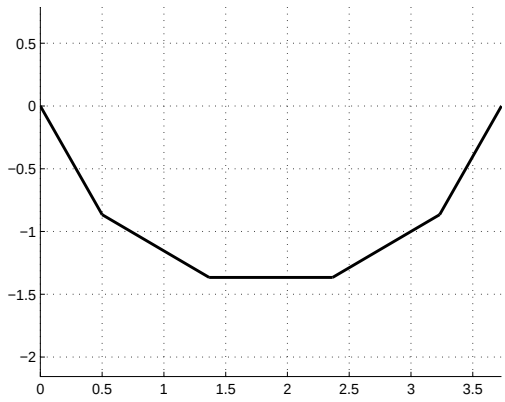

(a) Initial shape.

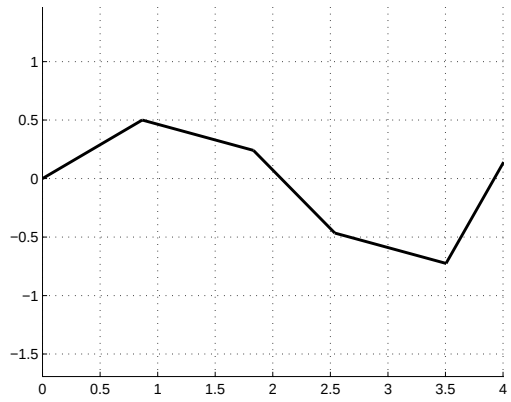

(b) Desired shape.

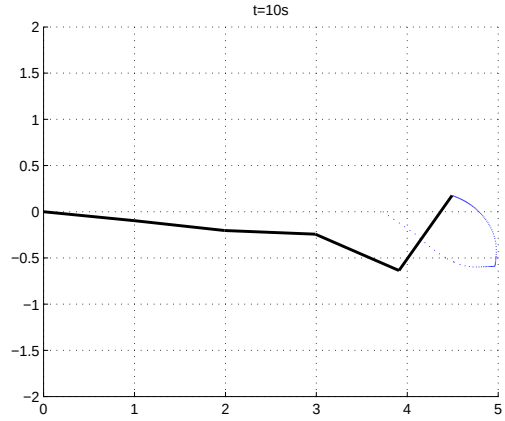

(c) Final shape attained.

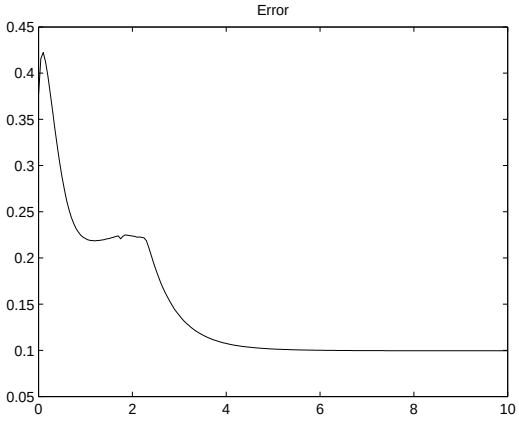

(d) Error.

Figure 4.1: Shape control example: Simulation result to achieve a sine curve with controlled gain matrix (5-segment).

4.2 Simulation Results

Figure 4.1(a) and 4.1(b) shows the initial shape and desired shape. As shown in Figure 4.1(c), the simulation result shows that the cable was not able to reach the exact desired shape (Sine Curve) but an approximation after a long time. Compared with Figure 3.12(b), the error curve shows in Figure 4.1(d) had less oscillations obviously. In addition, the error decreased in a faster rate and reached a smaller value (less than 0.1), which means the final shape is closer to the desired shape. These results confirmed that we could have a better performance on shape control by controlling the gain matrix.

Chapter 5

Conclusion

In this thesis, we have demonstrated a method for controlling the shape of a cable using force and position control of one of its ends. The motivation for such a system arises from tethered UAVs that get uninterrupted power supply trough a wired source. We simulate the wire in three dimensions and control the shape of wire with applying forces at the end of the wire. Moving forward, we would like to look into more effective simulation methods and control methods on the problem of shape control of a cable.

In Chapter 2, we have proposed a discrete model in three dimensions in order to obtain solutions numerically. Then we have derived the dynamic model of the cable in three dimensions from Lagrange's equations in this discrete model. Both force controlled system and position controlled system were developed to meet the needs in practice. We also conducted simulations to verify this dynamic model can achieve a good approximation to a real cable.

In Chapter 3, we have developed a controller to control the shape of the cable. This controller is based on the dynamic model in Chapter 3. With pseudoinverse, we can obtain the force we want to apply at the end of the cable to reach the desired shape. We have done the shape control simulation with gravity and without gravity. We have also considered the drag forces due to air in the simulation to find a more stable result of the shape control of the cable. All those simulations can verify that this controller could control the cable to

reach a satisfactory approximation to the desired shape.

In Chapter 4, we discussed the stability of the shape control problem. We have proposed the quasi-static discrete model to simplify the problem. We have derived the state error function and tried to find a gain matrix to marginally stabilize this system. By adjusting the gain matrix, we can have a better performance on shape control.

Under these efforts, we can apply this method to solve problems of shape control of a cable in some ideal and limited conditions. However, there are many practical challenges waiting for us to solve to improve the performance of this model and the proposed controller. In future, we plan to make further refinements to the proposed controller using novel methods, which can control the cable more precisely to attain a better approximation of the desired shape. We also plan to use a continuous dynamic model, which is more realistic but more complex than the discrete model. In addition, more factors need to be considered in the simulation and controller design, such as the friction, elasticity and the presence of physical obstacles in the environment. We also plan to perform shape control of a cable using two or more UAVs.

Bibliography

[1] Alain Goriely and Tyler McMillen. Shape of a cracking whip. *Physical review letters*, 88(24):244301, 2002.

[2] JL Jimenez, G Hernández, I Campos, and G Del-Valle. Newtonian and canonical analysis of the motion of a rope falling from a table. *European journal of physics*, 26(6):1127, 2005.

[3] Takayuki Matsuno and Toshio Fukuda. Manipulation of flexible rope using topological model based on sensor information. In *Intelligent Robots and Systems, 2006 IEEE/RSJ International Conference on*, pages 2638–2643. IEEE, 2006.

[4] Paweł Fritzkowski and Henryk Kaminski. Dynamics of a rope as a rigid multibody system. *Journal of mechanics of materials and structures*, 3(6):1059–1075, 2008.

[5] Pawel Fritzkowski and Henryk Kaminski. A discrete model of a rope with bending stiffness or viscous damping. *Acta Mechanica Sinica*, 27(1):108–113, 2011.

[6] Subhrajit Bhattacharya, Hordur Heidarsson, Gaurav S Sukhatme, and Vijay Kumar. Cooperative control of autonomous surface vehicles for oil skimming and cleanup. In *Robotics and automation (ICRA), 2011 IEEE international conference on*, pages 2374–2379. IEEE, 2011.

[7] Louis N Hand and Janet D Finch. *Analytical mechanics*. Cambridge University Press, 1998.

[8] Joao P Hespanha. *Linear systems theory*. Princeton university press, 2018.

[9] Gene H Golub and Charles F Van Loan. *Matrix computations*, volume 3. JHU Press, 2012.

[10] Roger A. Horn and Charles R. Johnson, editors. *Matrix Analysis*. Cambridge University Press, New York, NY, USA, 1986.

Vita

Bo Tian was born on April 28, 1994 in Beijing, China. His parents' names are Peishan Tian and Hongmei Ma. He graduated from Tsinghua University with his Bachelors of Engineering Degree in Automotive Engineering on July 2016. Then he attended Lehigh University, Mechanical Engineering and Mechanics Department on August 2016 to pursue a Master of Science Degree in Mechanical Engineering. He started his research under the direction of Professor Subhrajit Bhattacharya and finished this thesis on April 2018.